Załącznik 3

Emission of strange particles from symmetric nucleus-nucleus collisions at 2*A* GeV as the method to study properties of dense hadronic matter

Krzysztof Piasecki, Ph.D.

Self-review of research activities

Index

13.06.2016

K. Piasecki

I Single-topic cycle of publications constituting the main scientific achievement

[P1] K. Piasecki, … (FOPI Collaboration),
”Influence of ϕ mesons on negative kaons in Ni+Ni collisions at 1.91*A* GeV beam energy”
Phys. Rev. C 91, 054904 (2015).
Own contribution: 60% (participation in experiment and data calibration; data analysis, physics discussion, preparation of manuscript)
Impact factor (2015): 3.733

[P2] P. Gasik, K. Piasecki, … (FOPI Collaboration),
”Strange meson production in Al+Al collisions at 1.9*A* GeV”
Accepted for publication in Eur. Phys. Jour. A, arXiv:1512.06988
Own contribution: 30% (participation in experiment, data analysis, physics discussion, and preparation of manuscript)
Impact factor (2016): 2.736

[P3] K. Piasecki, … (FOPI Collaboration),
”Centrality dependence of subthreshold ϕ meson production in Ni+Ni collisions at 1.9*A* GeV”
Accepted for publication in Phys. Rev. C, arXiv:1602.04378
Own contribution: 50% (data analysis, physics discussion, preparation of manuscript)
Impact factor (2016): 3.733

[P4] K. Piasecki (For the FOPI Collaboration)
”Subthreshold ϕ meson production in nucleus-nucleus collisions”
EPJ Web of Conferences 71, 00109 (2014)

[P5] K. Piasecki (For the FOPI Collaboration)
”Strangeness production in heavy-ion collisions around 2*A* GeV in FOPI”
Jour. of Phys: Conf. Ser. 312, 022019 (2011)
Own contribution: 30% (preparation of manuscript, part of data analysis, and experimental results)

[P6] K. Piasecki (For the FOPI Collaboration)
”Properties of dense baryonic matter at 2*A* GeV”
Acta Phys. Pol. B 41, 405 (2010)
Own contribution: 30% (preparation of manuscript, part of data analysis, and experimental results)
Impact factor (2010) : 0.671

II Research activity after the Ph.D. as part of the FOPI Collaboration studies

1. Introduction[1]

1.1. Properties of nuclear matter at the beam energies between 1–2*A* GeV

The phenomena occurring during collisions of atomic nuclei at the beam kinetic energies T_b in the range of 1 – 2*A* GeV, where *A* denotes the mass number of the target nucleus, clearly exhibit the intermediate features compared to the adjacent regions of beam energy. The kinetic energies of the beam significantly exceed the energy of the Fermi motion of nucleons inside nucleus, and the corresponding de Broglie's wavelength drops down below the size of a single nucleon. In course of the collision (20–30 fm/*c*) the nuclear matter is heated up to temperatures in the order of 50–75 MeV, and undergoes compression to densities 2–3 times exceeding the ground state value ($\rho_0 = 0.17$ fm^{-3}) [1]. About 10 – 20% of nucleons becomes excited to the resonance states, e.g. Δ(1232), and the collision zone becomes the source of π mesons (cf. fig. 1), which are emitted in multiplicities reaching 30% of the number of nucleons participating in the collision. The collision zone also emits deuterons (reaching ¼ of the number of protons), light fragments, and other particles [2–4]. A still considerably high value of the baryon-chemical potential of the matter in the freeze-out state, $\mu_B \approx$ 700 – 800 MeV (cf. fig. 9; [5]), translates into the absence of the baryon antimatter production. The beam kinetic energies are insufficient for exciting the string degrees of freedom, and for the formation of the quark-gluon plasma (QGP). Only the lowest-lying excited states are being populated, and therefore the distribution of the populated states does not reach the continuum range.

Within the quantum chromodynamics (QCD) the nuclear matter in the normal conditions is characterised by breaking of the chiral symmetry. As a result, the hadron masses exceed many times the sums of masses of quarks which build them. With the increase of temperature and density the symmetry should be gradually restored [6]. According to the QCD-based models, already at the beam energy range of 1 – 2*A* GeV the expectation value of the condensate of quark-antiquark pairs should drop considerably (c.f. fig. 2), which should result in the modifications of effective masses

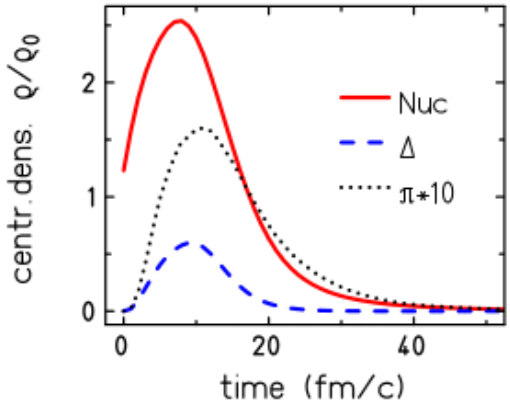

Fig. 1. Time evolution of density of nucleons, Δ resonances, and π mesons in the Au+Au collision at the beam energy of 1.5*A* GeV and impact parameter *b* = 0 fm in the framework of the IQMD model. Source: [1]

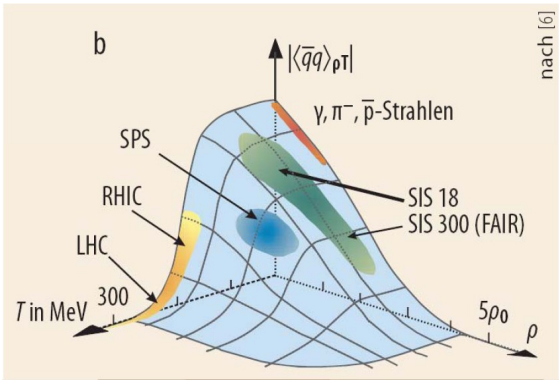

Fig. 2. Dependence of the the quark-antiquark condensate on temperature and density of the nuclear matter, as predicted within the QCD. Source: [14]

1 In this Summary a convention was applied that temperatures (or inverse slopes of the transverse momentum, and energy distributions) are given in terms of *kT* (and units of MeV or GeV).

and decay constants of hadrons traversing the hot and dense collision zone [7–13]. These changes should in turn modify the cross sections for production of these hadrons, and their interaction with surrounding particles. Various predictions of the modifications of kaon masses are collected in fig.3.

A specific feature of the considered range of energies is the onset of the production of particles with a strange valence quark, e.g. K and ϕ mesons, Λ and Σ baryons [15–17], and their lowest-lying excited states, e.g. K*(892) and Σ*(1385) [18,19]. Production of these particles occurs near or below the thresholds for their creation in the nucleon-nucleon (NN) collision in vacuum. Their appearance is possible thanks to the number of contributing effects: an extra energy stored in the Fermi motion of nucleons in nuclei, existence and specific properties of the multi-step channels leading to the production of a specific particle, as well as the abovementioned modifications of basic properties of hadrons in hot and dense nuclear matter [1]. The leading subject of the reported work is the subthreshold production of ϕ mesons and charged kaons.

1.2. Production of K^+, K^- and ϕ mesons in the collisions of heavy-ions at the energies around the NN threshold

Among the production channels initiated by two nuclei in the ground state (NN), the K^+ production process requiring the least energy is $NN \rightarrow NK^+Y$ (where the Y symbol stands for Λ or Σ hyperons), for which the threshold kinetic energy of the beam nucleon is 1.6 GeV. Due to the absence of antimatter in the entrance channel of the heavy-ion collision, a creation of K^- meson in a process similar to the one mentioned above is impossible. The energetically cheapest K^- production process with the NN pair in the entrance channel is $NN \rightarrow NNK^+K^-$, however, at the beam energies of $1 - 2A$ GeV it is a deeply subthreshold process ($T_{threshold} = 2.5$ GeV).

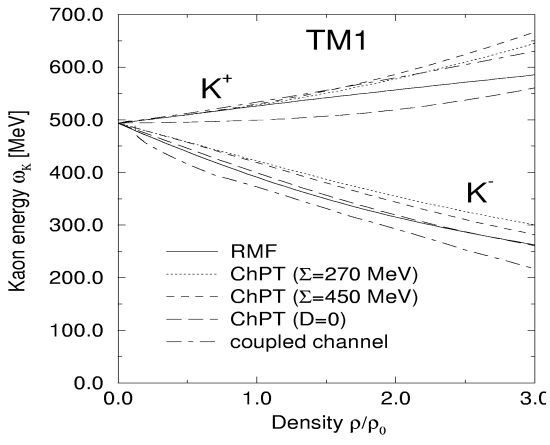

Fig. 3. Model predictions of the kaon energy (ω_K) at the vanishing momentum as a function of the scaled density ρ/ρ_0 of the surrounding nuclear matter ($\rho_0 = 0.17$ fm^{-3}). The U_{KN} potential is defined as $\omega_K - m_K$ difference for $\rho/\rho_0 = 1$. Source: [11]

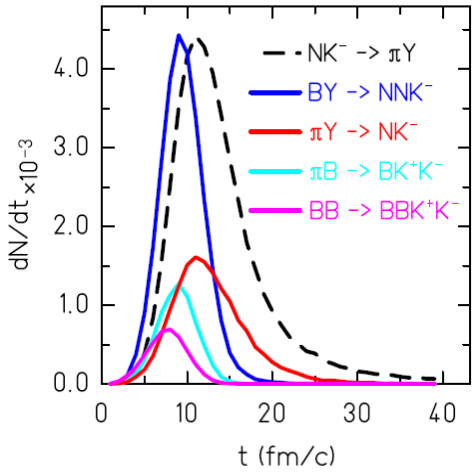

Fig. 4. Time evolution of the multiplicity density in the specific K^- production and absorption channels in the framework of the IQMD model. Source: [1]

An appearance of the K^- meson in course of the collision is, however, possible due to the interaction of hyperons and π mesons, which opens up the $\pi Y \rightarrow NK^-$ and $BY \rightarrow NNK^-$ channels (the so-called *strangeness-exchange* channels; $B \in \{N, \Delta\}$). Calculations in the framework of the BUU and IQMD microscopic transport models predict that the strangeness-exchange channels should be the leading K^- production process (cf. fig. 4), and the $\pi Y \rightarrow NK^-$ channel may also proceed via an intermediate resonance, $\pi Y \rightarrow Y^* \rightarrow NK^-$, where $Y^* \in \{\Sigma(1385), \Lambda(1405)\}$ [12,13]. The fact that the K^- production is possible only due to the multi-step process translates into considerably lower multiplicities of emission of these mesons in the collision compared to the multiplicity of the positively charged kaons: in the considered energy range the ratio of K^-/K^+ yields is at the level of 1 – 3 % [15].

The ϕ meson is a particle with the strangeness number S = 0, whose valence quarks are exclusively strange: s and $\bar{s}$. A production of this meson at the beam energies of 1 – 2*A* GeV occurs also deeply below the threshold in the $NN \rightarrow NN\phi$ channel ($T_{threshold}$ = 2.6 GeV), therefore this meson is produced in the multi-step channels and/or thanks to an additional momentum of the Fermi motion of nucleons. However, the experimental data on the production of this meson were so scarce, that they did not allow for identification of the dominant production channels. At the beginning of my studies only one measurement of ϕ mesons at the beam energies of $T_b < 10A$ GeV was available. A registered sample originated from the central collisions of Ni+Ni at the energy of 1.93*A* GeV, and amounted to mere 23 ± 7 reconstructed ϕ meson events. Basing on this sample, the yield of ϕ mesons was estimated to be around $1–4 \times 10^{-3}$ per triggered event, thus the result was burdened with large uncertainty [16]. The issue of the ϕ meson production will be discussed in the further parts of the current chapter.

Studies of scattering of K^+ on nucleon have shown that this process is characterised by a relatively low cross section and low absorption. It translates into a relatively long mean free path of a kaon in the nuclear matter (about 5 – 7 fm for kaons with momenta below 0.7 GeV/*c* in the matter at normal nuclear density, $\rho = \rho_0$, [21]). Taking into account that the mean lifetime of a kaon is much longer than the duration of the collision, these properties render the K^+ a suitable probe of the collision zone. Investigation of kaon-nucleon scattering points to the repulsive nature of the K^+N interaction [20–22]. In the context of the dynamics of K^+ meson in the collision zone of heavy-ions, within the simplest approaches the modifications of properties (e.g. of the effective masses) are parameterized by the kaon-nucleus potential (U_{KN}). This potential can be defined as the difference between the kaon energy and its mass in vacuum at normal nuclear density ($\rho = \rho_0$). If the interaction is repulsive (attractive), the U_{KN} is positive (negative). A repulsive nature of the K^+N scattering translates into the positive potential ($U_{K+N} > 0$) associated to the positively charged kaon traversing the nuclear matter, which also means an increase of the effective mass of this particle. The K^+ mesons undergo pushing out of the centers of density of the matter in which they were produced [1,12,22]. A systematics of various model predictions on the dependency of the kaon energy on density of surrounding nuclear matter is shown in fig. 3.

The properties of K^- mesons are different. Scattering of these particles on the nucleon is characterised by the relatively large cross section; the interaction is attractive, and the absorption occurs [20,23]. Indeed, one of two dominant production channels of negative kaons, $\pi Y \rightarrow K^-N$, can easily proceed in the nuclear matter in an opposite direction: $K^-N \rightarrow \pi Y$, which causes the disappearance of this kaon. It is demonstrated e.g. by the dashed curve in fig. 4, which presents the results of simulation of Au+Au collision at 1.5*A* GeV within the IQMD transport model [1]. According to the models predicting the modifications of antikaon properties in the nuclear matter, an attractive nature of the $\bar{K}N$ interaction translates into the considerably negative potential ($U_{K-N} < 0$) associated to the motion of this particle inside the matter. In other words, the effective mass of the antikaon decreases [1,9,13,22; cf. fig. 3].

These effects influence the dynamics of kaons, and thus they show up in their energy distributions, and collective flows. One of the aims of our study was the reconstruction of the charged K mesons kinematic distributions. An extraction of information on the scale of U_{KN} potentials requires a comparison of the experimental given distribution with the predictions of the microscopic transport model. However, the effects of the modifications of properties of particles are not the only factor influencing the profile of the distribution: the concurrent phenomena are the scattering and absorption of kaons (mainly on nucleons) [1]. Therefore, in order to extract, within the specific model, the change of profile due to the non-vanishing U_{KN} potential, one should compare the predicted profile with the one obtained when the modification effects are switched off. In case of K^- mesons such calculations encounter an additional conceptual difficulty, related to the ϕ meson production and its dominant decay channel.

The mean free path of the ϕ meson is $c\tau = 46$ fm [20]. From a comparison of this value with an average duration of the nuclear collision, amounting to about 20–30 fm/c, one may conclude that most of these mesons decay outside the collision zone, thus in vacuum. A dominant ϕ meson decay channel is the $\phi \rightarrow K^+K^-$ process (branching ratio BR = 48.9%). Taking into account that the multiplicity of K^- mesons emitted in the collision of heavy ions is much lower than that of the positive kaons, the di-kaon decays of ϕ mesons may constitute a considerable contribution to the total production of K^- mesons, competing with the direct emission from the hot and dense collision zone. Apart from differences in the surrounding medium, these two groups of negative kaons are also characterised by the contrary kinematic conditions. For the di-kaon decay of the ϕ meson, a small difference between the masses of the substrate and products ($m_\phi c^2 - 2m_K c^2 = 32$ MeV) translates into low kinetic energies of negative kaons: for the ϕ mesons emitted from the NN center of mass frame with the temperature of about 100 MeV the energy distribution of the daughter negative kaons is characterised by temperature of about 60 MeV. The latter value is lower than most of the experimentally obtained inverse slopes T [2] of the energy distributions of kaons [15]. One can therefore suppose that for the energy distribution of the negative kaons the contribution from the $\phi \rightarrow K^+K^-$ decay channel is „colder" than that from the kaons emitted directly from the collision zone. A determination of the weight of the $\phi \rightarrow K^+K^-$ process becomes crucial in this context. If it turned out to be meaningful, then within the investigation procedure of the U_{K-N} potential by comparison with the experimental K^- distribution, the model calculation would have to contain the proper description of the ϕ meson emission both in terms of the cross section and kinematical characteristics. In turn, if the specific model calculations did not account for the ϕ meson production, than the abovementioned contribution should be subtracted from the experimental K^- meson distributions. One of the goals of my research was the determination of weight of this contribution, and its kinematical characteristics for a couple of systems of colliding heavy ions.

One of the clearly observed effects in the heavy ion collisions at the beam energies of about $1 - 2A$ GeV is the larger values of the inverse slopes of energy distributions of positive kaons, $T(K^+)$, compared to those of negative kaons, $T(K^-)$ (cf. fig. 10). According to the calculations in the framework of the IQMD model the main cause of this effect may be the abovementioned in-medium modifications of properties of kaons: the opposite signs of the U_{K+N} and U_{K-N} potentials translate into an increase (K^+) or decrease (K^-) of the mean kinetic energy of kaons in comparison with the default distributions (for the vanishing potential), the latter ones predicted to be very similar to each other [1]. However, due to the admixture of the ϕ meson decay products to the spectrum of negative kaons, a doubt arose whether a part of difference between $T(K^+)$ and $T(K^-)$ may originate from these decays. A search for an answer to this question was also the goal of my work.

2 If the energy spectrum of emitted particles or their transverse momentum spectrum for a narrow rapidity interval can be parameterized by the function proportional to $\exp(-E/T)$ or $\exp(-p_T/T)$, the T parameter is dubbed the "*inverse slope*" of this distribution.

At the beginning of my studies only one result of the ϕ meson production, based on 23 ± 7 events was available. The unavailability of the ratio of ϕ/K^- yields, and the energy and angular distribution of ϕ mesons (or K^- originating from their decays) did not allow for determination of the two abovementioned sources of K^-. An absence of data translated into an unacquaintance within the transport models of the production mechanism of ϕ mesons in the nuclear matter, and thus the resulting cross sections. In the review paper [1] devoted to the strangeness production in the framework of the IQMD model, the production of this meson was not included at all, and in particular the influence of this meson on the extraction procedure of the K^- potential in the nuclear matter from the phase space distributions was omitted. In case of the BUU model [12], and the most recent predictions of the UrQMD model [24] the production of ϕ mesons was accounted for in the calculations, however these approaches assume the diametrically different underlying mechanisms. Within the BUU model the BB and MB (B = baryon, M = meson) channels we assumed to be the dominant ones, whereas within the UrQMD approach the ϕ mesons were mainly produced via the deexcitations of the series of heavy nucleonic resonances (with masses around 2 GeV/c^2) to the ground state.

The first experimental analysis basing on a sample of about 168 events from the Ar+KCl collisions at 1.76*A* GeV was published in 2009 by the HADES collaboration [25]. It was determined that 18 ± 7 % of negative kaons originate from decays of ϕ mesons. Calculations in the framework of the BUU and UrQMD models gave results in agreement with the experimental findings within the uncertainties, both in terms of the ϕ meson multiplicities, and the ratio of ϕ/K^- yields, regardless from the abovementioned differences in the proposed production mechanisms. It has become crucial to find the ϕ meson production yields, and their contributions to the K^- emission for the other heavy ion systems, in particular for those where the analyses of the in-medium properties of K^- mesons were performed (or published).

1.3. Global parameters of the heavy-ion collisions: the thermal model

One of approaches aimed at description of the emission of particles from heavy ions is the thermal model. Within this approach one assumes the thermal and chemical equilibrium of the system, which is described by parameters: T (temperature), μ_B, μ_S, μ_{I3}, (baryochemical, strangeness, and isospin potential, respectively), where the values of μ_S and μ_{I3} are fixed by the conditions of the initial state [25]. Experimental reconstruction of the collection of yields (or yield ratios) of emitted particles allows for comparing them with the predictions of the thermal model and extraction of the T and μ_B parameters. Results from the series of systems and beam energies plotted on the $T - \mu_B$ phase diagram suggest a monotonic dependency between these parameters (cf. fig. 9).

For the range of beam energies delivered by the SIS18 accelerator in GSI, Darmstadt, currently there is no consensus on whether the thermodynamical equilibrium is reached in course of the collision [28,29]. However, one can consider the thermal model as a functional parameterisation, which usually predicts the emission yields after the chemical freeze-out quite well, employing only 2–3 parameters. Another specific feature of 1 – 2*A* GeV beam energy region is the low multiplicities of emitted particles with the strange quark. For this reason, in the majority of relevant papers it is additionally assumed that the strangeness number S is conserved exactly (and not on average) in each event, which implies an application of the canonical ensemble for the description of this group of particles. In some other versions of the model it is assumed that in the sector of particles containing at least on strange quark the chemical equilibrium is not reached, which results in the deficit of their multiplicities, parameterised by the γ_s exponent ($\gamma_s < 1$ for the deficit) [30].

One of the goals of my research was the enhancement of the list of known yields of particles emitted from the Al+Al and Ni+Ni collisions at the energy of 1.9*A* GeV and comparison of them to the predictions of the thermal model, obtained with help of the dedicated THERMUS package [31]. Results of this analysis are reported in the Subsection 5.3 of the present Summary.

2. FOPI spectrometer and the selected experiments

2.1. FOPI setup

The FOPI experimental setup was the modular spectrometer of charged particles, installed at the SIS–18 accelerator at the GSI facility in Darmstadt (Germany), and being in operation in years 1990 – 2012. It acquired the experimental data from the heavy-ion collisions at the beam energies in the range of 0.1 – 2.0*A* GeV, and collisions involving the proton and π^- beam. The FOPI setup, shown schematically in fig. 8 was designed for the measurement of charged particles (hadrons, and light ions) and these neutral particles which decay inside the detector into the charged products. The modules of FOPI were characterised by the full or approximate azimuthal symmetry with respect to the beam axis. The Start detector was mounted on the path from the beam pipe to the target. It signalled the moment of passage of the beam. The CDC drift chamber (Central Drift Chamber) was placed around the target, and the Helitron drift chamber was mounted at forward polar angles. The Time-of-Flight (ToF) detectors were placed around these chambers: the Plastic scintillation Barrel, in the geometry of the cylinder's lateral plane, surrounded the CDC, and after year 2006 an additional device dubbed MMRPC, and designed in a similar geometry, was additionally installed. The Forward scintillation Wall was mounted behind the Helitron. Within this wall, the Zero Degree detector was placed at innermost polar angles, and the Plastic Wall (PlaWa) detector was mounted more outside. The whole FOPI spectrometer covered a considerable part of the momentum space of particles emitted from the heavy-ion collision zone. Details on the construction and characteristics of this setup were described in refs. [32,33].

In the following I will focus on the part of detection modules which I used for the particle reconstruction in the presented analyses. The CDC and the surrounding ToF detectors were placed inside the magnet solenoid of the field strength of 0.6 T, thus causing the charged particles to follow the track of a helix with the radius proportional to the transverse momentum. If a charged particle passes through a given drift chamber, it activates the signals in the readout wires close to the particle's track. A dedicated software (so-called ”*tracker*”) was reconstructing the tracks of particles

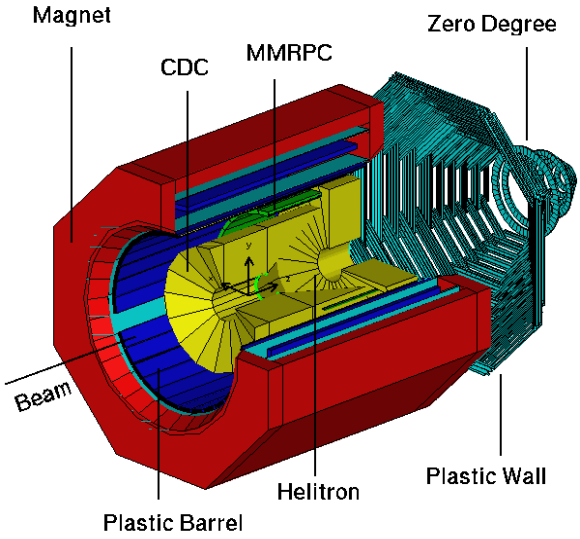

Fig. 5. Electromagnetic FOPI spectrometer within the configuration applied in years 2007 – 2010.

basing on the collections of signals stored on disks. A part of particles was additionally passing through the Time-of-Flight detectors, generating the signal at the place of hitting, which was registered at both ends of the long scintillation crystal. This signal in a coincidence with the Start detector information determined the Time-of-Flight (ToF) of a particle, whereas a measurement of the track of particle's flight allowed to reconstruct its velocity.

The charged particle identification procedure in the CDC was being performed by correlating the particle's momentum with its specific energy loss in gas. However, for the charged kaons, the statistical scatter and closeness of the minimum ionisation region, this method was by far insufficient. In this case an use was made of particles leaving signals in one of the ToF detectors. It yielded an additional information on velocity, which made possible the identification of particles based on the relativistic formula $p = m\gamma v$. However, the range of charged kaons' momenta where the separation of particles was possible, depended on the time resolution of the ToF detector. For the Plastic Barrel this range was reaching the limit around momentum of 0.55 GeV/c (0.38 GeV/c) for K^+ (K^-) [33,34,P2], which was clearly narrowing down the insight into the kinematical distributions of those kaons. For this reason the FOPI collaboration has constructed and installed in year 2007 the new ToF detector, dubbed Multi-strip Multi-gap Resistive Plate Chamber (MMRPC) [35,36]. The Section 4 of this Summary will be devoted to this detector. Much better resolution of this device allowed for a broad widening of the momentum range of kaon identification [37,P1], which also strongly enhanced the capabilities of studying the $K^{\pm}$ and ϕ meson production performed by our Collaboration.

2.2. Selected experiments performed by the FOPI Collaboration

During my cooperation with the FOPI research group I participated in all its experiments. They were put together in Table 1.

Table 1. Experiments of the FOPI research group in years 2005 – 2010

Symbol of experiment	Configuration	Beam kinetic energy per nucleon (T/A) or beam momentum (p) [GeV]	Date of experiment
S279	Al+Al	T/A = 1.91	08.2005
S325 / S325e	Ni+Ni	T/A = 1.91	09.2007 and 03.2008
S338	Ni+Pb	T/A = 1.91	01.2009
S338R	Ru+Ru	T/A = 1.93	02.2009
S349	p+p	p = 3.1	06.2009
S339	π^- + p	p = 1.7	06.2010

Due to the expansion of the accelerator at the GSI to the SIS–100/300 phases and new site management, the FOPI detector was dismantled in year 2012. However, during the last 3 years of its operation data from four experiments was acquired, in which I actively participated. A part of this data still is to be analysed, which is the task I plan to participate in.

2.3. Centrality class of heavy-ion collisions

Phenomena occuring during the heavy-ion collision depend on a degree of centrality. The latter is usually strongly correlated with the multiplicity of particles emitted outside the narrow solid angle around the beam axis. By covering a considerable part of the full solid angle, the FOPI setup detected a majority of emitted charged particles. During experiments the trigger system counted the multiplicity of hits in the modules of PlaWa and ToF detectors. By comparing these multiplicities with the predefined threshold values, the trigger system was generating the decision on the acquisition of an event, as long as the system was not blocked due to storing procedure of a previous event. An off-line data analysis allows for the elimination of events originating from outside the target or with information stored improperly, and for the determination of the total number of accepted events. One of the methods of centrality class determination is the extraction of a fraction *f* of the reaction cross section by dividing the number of accepted events by the number of beam impulses obtained from the Start detector, the latter multiplied by the probability of interaction of a beam ion with the target. In the next step, within the ”sharp cut-off” model one determines the cross section σ_{exp} , and the maximum impact parameter, which correspond to the pre-set threshold value of a trigger. Finally, within the parameterisation of the collision as an interpenetration of sections of balls [27], an average number of nucleons participating in the collision (so-called ”*participants*”, $\langle A_{part} \rangle_b$) is determined .

My contribution consisted in determination of the fractions *f*, the values of σ_{exp} and $\langle A_{part} \rangle_b$ for the S279, S325(e), and S261 experiments (the latter is one of the earlier experiments whose data I also analysed).

3. Efficiency calculations

For the most of analyses of the phase space and determination of yields of particles detected by the FOPI setup, it is necessary to construct the detection efficiency maps. The FOPI group has developed the simulation environment based on the GEANT3 package [39], where all the subdetectors were mapped in details. Within this environment a file of events is given as input, where each of these events is the result of simulation of particle emission from a heavy-ion collision based on the microscopic transport model, eg. IQMD [1]. Particles emitted with a low multiplicity in an event (e.g. K^+, K^-, and ϕ mesons) are generated separately based on the Boltzmann distribution with an optional anisotopic modification of the angular distribution, and appended to the collection of particles from an event generated by the IQMD code. For the particles emitted with high total multiplicities in a collision, their distribution may still exhibit shortages in some regions of phase space (e.g. parameterized in the $p_t - y$ frame). In such cases one can add to a present contribution a constant „pedestal”, in other words one can generate particles from the homogeneous distribution in given coordinates and add them to the existing sample. The simulation package is responsible for tracing the tracks and description of interactions of all the particles originating from the generated collection of initial particles. For each event, a collection of particles is transported from the vertex through the volume of the experimental setup. As particles traverse the detectors, they leave traces appropriate for the detection processes in these devices. These traces are digitised and stored in an output file according to the same format, as used for the data generated by the acquisition system during the real experiment. In the next step the simulated data is subject to the same tracking and particle identification procedures, as for the true experimental data. By comparing for a given observable *x* an obtained distribution with the initial one, one obtains the detection efficiency, $\varepsilon(x)$, of a given particle in a specific detector.

Within the analyses of data from the experiments of the FOPI collaboration I performed the full efficiency calculations for the detection of protons, deuterons, and π^+, π^-, K^+, K^-, and ϕ mesons

from the S325(e) experiment; protons and deuterons from the S279 experiment, and the ϕ mesons from the S261 experiment (central Ni+Ni collisions at the beam energy of 1.93*A* GeV, year 2003). For the ϕ and K^- mesons from the S325(e) experiment the calculations are presented in Section IV and in fig. 3 in ref. [P1]. A determination of efficiency of ϕ mesons from the S261 experiment was described in Section IV of ref. [P3]. An information about performing the efficiency calculations for the detection of protons and deuterons from the S279 experiment can be found in report [26]. Regarding the measurement of protons, deuterons, π^+, and π^- mesons in the S325(e) experiment a determination of the efficiency with help of the abovementioned method was the condition for extracting the internal efficiency of ToF (MMRPC, and Plastic Barrel) detectors, which will be reported in Subsection 4.2 of the present Summary. The K^+ meson detection efficiency was presented hitherto only at the FOPI collaboration meetings.

A key condition for correctness of the efficiency determination procedure is the adjustment in the simulation package of the control parameters, characteristic for each of utilised detector, to their values in a real experiment, as well as of all the other parameters of further analysis. For instance, for the CDC one has to adjust among others the values of: velocities of an electron drift in gas, resistance of the readout wires, parameters of the mass identification on the plane correlating the specific energy loss with the particle's momentum. In turn, for the ToF detectors, subjected for comparisons are the distributions of transverse and longitudinal component of a vector of difference between the point of particle hit in the detector module, and the expected hit based on an extrapolation from the reconstructed track in the CDC. A comparison of distributions of these variables for the simulated and true data exhibits minor deviations, difficult to remove, which implies that the cuts on the values of these parameters applied to the collections of particles (tracks) in both types of analyses may not bear identical results. In this case, a correction procedure consists in finding such boundary values of the abovementioned control distributions for the simulated data, that the cutting conditions are satisfied by the same percentage of tracks, as for the set of true experimental data.

A special case of this procedure is the stage of comparison of the mass parameters. FOPI utilises two methods of identification of particle's mass. Within the first one, that bases on data from the CDC, the m_{CDC} mass parameter is extracted by fitting the Bethe-Bloch formula to the point on a correlation plane between specific energy loss and momentum of a particle. The other method is possible at the presence of an additional information from the ToF detector, and consists in finding the m_{ToF} mass parameter by inserting the momentum and velocity of a particle into the relativistic formula $p = m_{\mathrm{ToF}}\,\gamma v$. Both parameters are characterised by statistical scatter, which intensifies with the particle's momentum. In case of analyses of charged K, and ϕ mesons in the K^+K^- decay channel, for the kaon identification it is necessary to investigate the two-dimensional distribution of mass parameters, $m_{\mathrm{CDC}} - m_{\mathrm{ToF}}$. Due to the increase of scatter with the particle's momentum, this distribution is inspected for consecutive slices of momentum. In addition, the signal of interest is situated on the slopes of signals originating from particles of adjacent masses: it is the case especially for higher momenta, and for the Plastic Barrel detector, where the resolution for a given momentum is worse than that for the MMRPC. The identification procedure of kaon candidates is based on applying cuts on the $m_{\mathrm{CDC}} - m_{\mathrm{ToF}}$ plane for consecutive slices of momentum. At the same time, setting up specific cuts results in rejection of some fraction of particles of interest. In order to correctly account for this loss of kaons, also the sample of simulated data must be subject to appropriate cuts on the $m_{\mathrm{CDC}} - m_{\mathrm{ToF}}$ plane. However, an irremovable drawback in the simulation procedures of the CDC response within the GEANT3 environment is the partial difference of profile of the m_{CDC} distribution from that for the real experimental data. In consequence, the procedure of the adjustment of mass cuts for the simulated data to those applied for the real data requires particular care.

In case of study of ϕ mesons in the K^+K^- decay channel from the S261 experiment I applied a somewhat modified approach, which was reported in Section IV of ref. [P3]. The goal of this approach was to obtain for each slice of momentum of kaons in the real data, an information on the fraction of kaons rejected by the mass gates, and subsequently to apply to the simulated data the rejection probability equal to the fraction found. For this reason I fitted the two-dimensional Gaussian function to the distribution of kaons, and obtained the fraction of area under this function for the region remaining outside the mass gates. However, I did not limit this approach to the slices of momentum where the distribution of kaons on the plane remains uncontaminated by the slopes of distributions originating from particles with neighbouring masses (π mesons, and protons). For higher momenta, where such a contamination was observed, but still limited to some subregion on the $m_{CDC} - m_{ToF}$ plane, I identified the subregion free from contaminations, and fitted the Gaussian function exclusively within the latter range. It allowed for enhancement of applicability of the presented method to somewhat higher momenta, especially for the K^- mesons.

All the experimental results reported in Section 5 of the present Summary were obtained with help of the efficiency corrections described above.

4. The MMRPC Time-of-flight detector at the FOPI setup

A limitation of the idenfitication capability of charged kaons to the low momenta, which was mentioned in Subsection 2.1, was the result of rather poor time and position resolution of the Plastic Barrel Time-of-Flight detector ($\sigma_t \approx 250$ ps, $\sigma_\phi \approx 0{,}7°$). The MMRPC detector, installed in years 2000 – 2007 featured much better resolution: $\sigma_t \approx 70$ ps (after excluding the Start detector's resolution), $\sigma_\phi \approx 0.17°$. A better position resolution was possible thanks to the increase of granularity from 180 to 2400 active strips. However, this enhancement intensified the necessity for a precise synchronisation of the calibration parameters [35].

My work related to the MMRPC detector was focused on four issues:

– cooperation on the precise calibration of the new detector and removal of bad signals,

– implementation of the MMRPC detector in the GEANT3 simulation framework (defining the geometry of the components and the authorship of the signal digitisation procedure),

– determination of an internal detector efficiency due to its inhomogeneous position and momentum responses to the traversing charged particles,

– determination of the differential and total efficiency of the CDC–MMRPC system for protons, deuterons, and K^+, K^- and ϕ mesons from the S325(e) experiment.

The first two issues were only reported at the internal meetings of the FOPI Collaboration in year 2008. They were the necessary preparations for the analyses that I performed on the properties of emission of $K^\pm$ and ϕ mesons from the S325(e) experiment, where the MMRPC detector was first installed, however they were not reported in the papers constituting the presented cycle. For this reason, below I will present in short the scheme of implementation of the MMRPC detector geometry, and the signal digitisation procedure within the GEANT3 framework.

4.1. Implementation of the MMRPC detector within the FOPI simulation environment

The first step of the implementation of the MMRPC detector was the mapping of its geometry. The detector was made in form of the side area of a cylinder of radius of 97 cm (cf. fig. 6a), around which 30 so-called ”super-modules” of length of 90 cm were installed. Each ”super-module” was filled with the gas mixture and housed 5 detection modules (cf. fig. 6b). A single detection module was composed of the stack of electrode plates separated by small gaps (cf. fig. 6c). A middle plate functioned as an anode and was composed of 16 equidistant, conductive strips. An anode was sandwiched by stacks of cathodes made of highly-resistive glass. A particle passing through the given module was ionising in its body the atoms of gas. A primary charge was moving in the high electric field, and thus was generating the secondary avalanche. Highly-resistive electrodes were quenching the propagation of an impulse over the whole area of the plate, whereas the charge was collected by conductive strips mounted on an anode. My task consisted in an implementation of the geometry of the MMRPC detector in an appropriate procedure, and storing it in the data structure based on the fortran-based ZEBRA package.

In the next step I programmed the signal digitisation procedure, i.e. an algorythm converting the information on position and time of a particle hitting the active element of the detector into the distribution of charge at the sides of 16 strips. Within the model in the first step I assumed an addition of a small, given noise to the time information of a particle's hit. The charge of a given amplitude was subsequently dispatched to 16 anode strips, according to the spatial Gaussian distribution with a value of dispersion defined by the user. An assignment of charge was done under condition that the charge attributed to a given strip passes the given threshold value (cf. fig. 7a). Values of dispersion and threshold charge were chosen such that they corresponded to an average size of a cluster observed in real FOPI experiments (about 3 – 5 neighbouring active strips). Considering the longitudinal view of an anode, the particle's hit position was distorted by the Gaussian function of width corresponding to the experimentally observed spread (about 2 cm). Subsequently, each of charges was propagated towards two ends of a given strip in a longitudinal section (cf. fig. 7b) with a given velocity of charge propagation (about 15 cm/ns). Within the model the user was also in disposal of a possibility of signal attenuation along the strip. A set of charge signals formed in this way was stored in an accepted by the FOPI group format of a general experimental data acquisition structucture, based on the ZEBRA package.

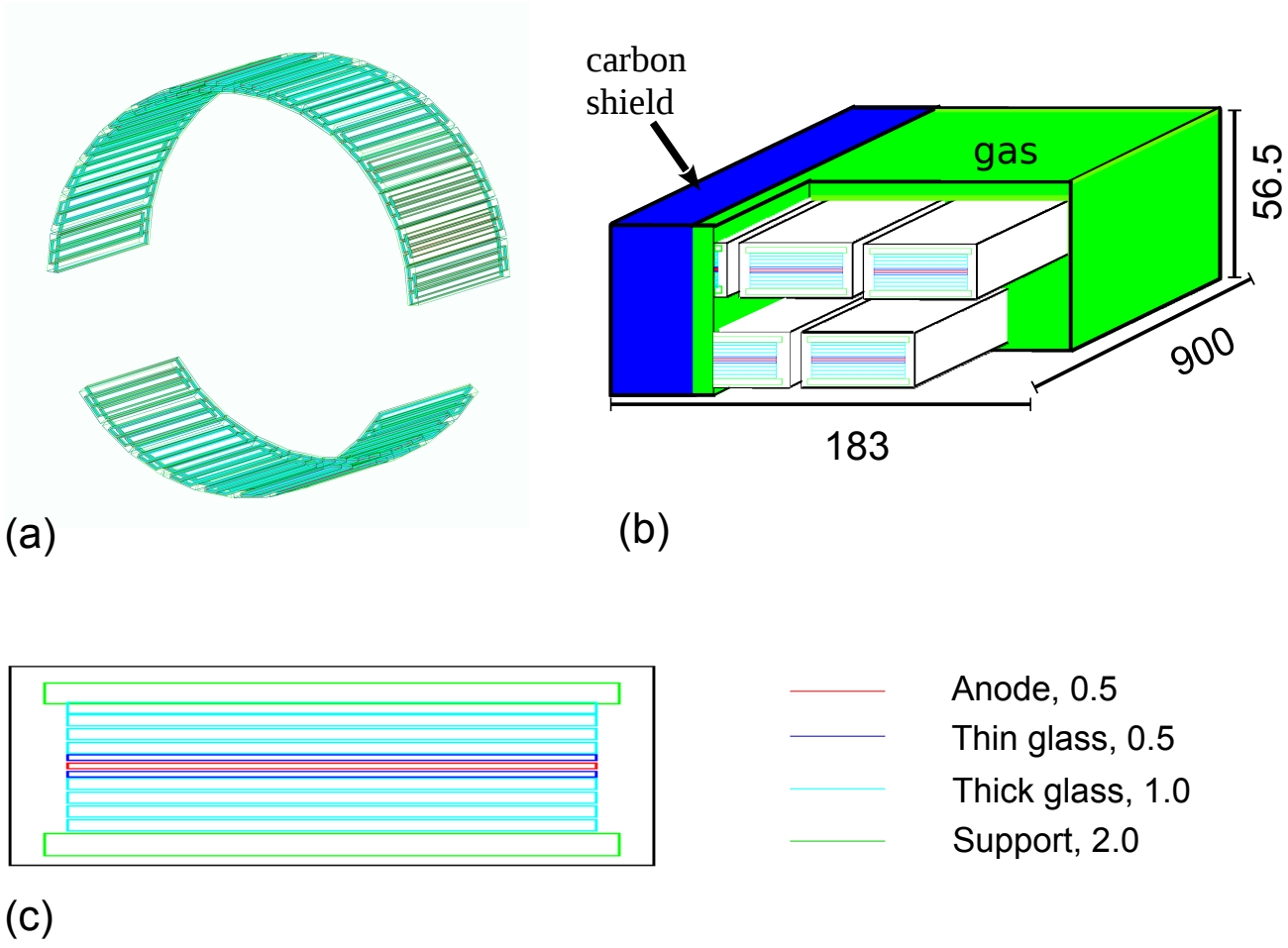

Rys. 6. Mapping scheme of the MMRPC structure in the GEANT3 simulation environment. (a) Spatial arrangement of super-modules. Empty space is due to the mounting rail of the detector, and absence of 4 super-modules in the FOPI's S325 experiment. (b) Arrangement of modules in a single super-module. (c) Section through the single module. Dimensions are given in mm.

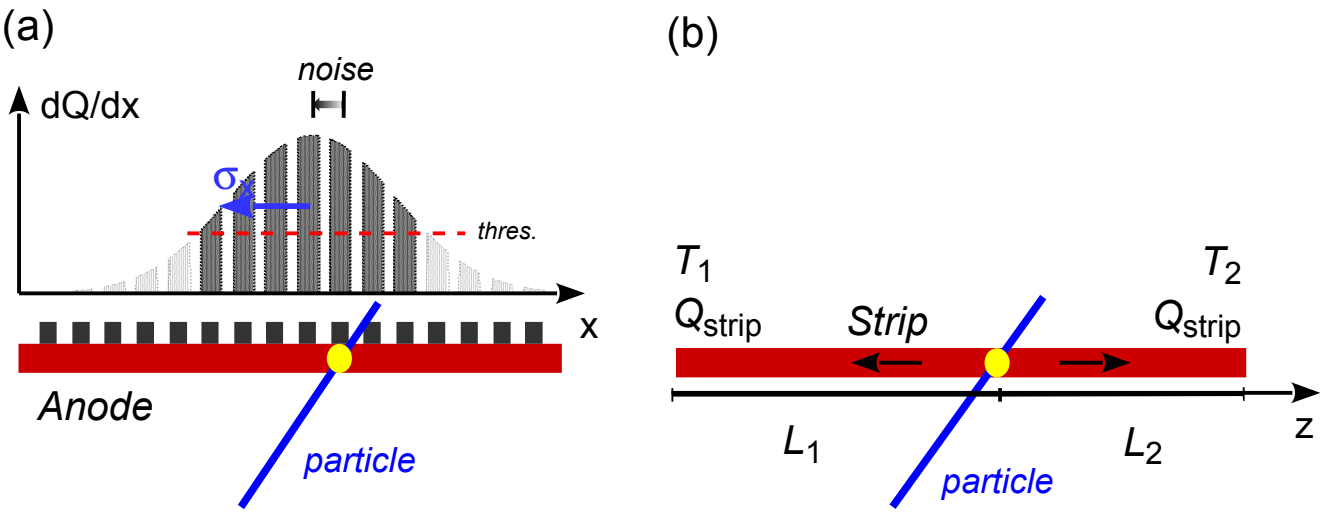

Rys. 7. Scheme of signal digitisation by the MMRPC detector in the GEANT3 simulation environment. (a) Transverse, (b) longitudinal section across the anode at the place of particle's hit. Explanation of the digitisation procedure can be found in text.

4.2. Internal efficiency of MMRPC detector

In course of the analysis of the transverse momentum distributions of protons and charged kaons identified with help of the CDC and MMRPC I noticed, that the inverse slopes of the kaon transverse momentum spectra (corrected for the hitherto available detection efficiencies) reach the values of about 20 MeV smaller than the ones expected from the available systematics (cf. fig. 20 in ref. [15]). In addition, the distribution of inverse slopes as function of rapidity for protons measured by the CDC–MMRPC tandem of detectors was characterised by a different profile compared to that for the same particles, but obtained with help of the CDC only.

In light of these observations I put forward the hypothesis that the MMRPC detector is biased with an internal, inhomogeneous efficiency, unaccounted for in the hitherto obtained efficiency calculations. In order to determine it, I assumed that out of particles registered as tracks in the CDC, a fraction of those leaving further a hit in the MMRPC detector is not identical within the experimental data and the one simulated within the GEANT environment. A range of this deviation depends in general on the position of a hit in the MMRPC (parameterised by the polar angle ϑ with respect to the target) and the transverse momentum p_T of a particle and on a type of hadron in question. I also verified that the difference in efficiencies does not depend on the azimuthal angle ϕ. A problem of the inhomogeneous position efficiency of the MMRPC can be seen in an unequal profile of the position distribution of particle hits in the lower panel of fig. 12 in ref. [35], however this effect was not investigated therein.

In order to quantify the inhomogeneities, in the first step I identified particles of a given type (selected were: protons, deuterons, π^+, and π^- mesons) both in the experimental and simulated data sets. Next, for each of these sets I determined the fraction f of tracks having the time information in the MMRPC out of all the tracks registered in the CDC, observed as function of ϑ and p_T . If the experimental efficiency of the MMRPC detector was exactly reconstructed by the GEANT environment, then the distributions of the abovementioned fraction as a function of ϑ and p_T for the experimental (f_{exp}) and simulated (f_{sim}) data would have identical profiles and levels of normalisation. In such a case the ratio of these fractions, defined as $\varepsilon^{ToF} = f_{exp} / f_{sim}$ would equal to 1 for every value of ϑ and p_T. In any other case, the ε^{ToF} would be the measure of an internal efficiency of the MMRPC detector, unaccounted for in the GEANT environment.

The analysis of ε^{ToF} function has revealed deviations from the value 1, and its clearly inhomogeneous profile for each type of selected particles. Full results of this analysis were presented at the meetings of the FOPI group, whereas the idea of extraction of ε^{ToF} was described in Section IV B of ref. [P1], and fig. 3d therein presents the results for the sample of protons. It can be seen on this plot, that ε^{ToF} is inhomogeneous, exhibiting variations within 0.8 – 1.1. During the analysis I also found that that for different types of particles the profiles of ε^{ToF} were nearly identical, however the levels of these functions differed by about 5 – 15 percent points depending on a pair of compared particles. I also checked the profiles of ε^{ToF} for the CDC – Plastic Barrel tandem of detectors. A result of this analysis for the data from the S325(e) experiment is presented in fig. 3c of ref. [P3]. It can be seen, the profile of ε^{ToF} is nearly flat, but at the same it exhibits about 13% drop of the true efficiency with respect to the one obtained from the simulations. Thus, thanks to this analysis another information was extracted, that the detection efficiency of the Plastic Barrel in this experiment was somehow lower than that obtained by hitherto applied simulation procedures. I performed the analysis for the CDC – Barrel detectors for the data from the S261 experiment as well, which is presented in Section IV of ref. [P3], and the results for π^- mesons and an inclusive sample of π^+ and protons is ilustrated in fig. 3 of that paper.

The presented method of determination of the internal efficiencies of the ToF detectors was applied in the procedure of the reconstruction of phase space distributions and yields of K^+, K^-, and ϕ mesons. It should be also clarified that due to relatively low statistics of measurement of these mesons and an inability of their identification within the CDC only in a broader range of momenta, it is not possible to obtain the ε^{ToF} efficiency profiles directly for these particles. For that reason, the maps of ε^{ToF} were obtained from samples of particles measured with high statistics (protons, deuterons, π^-, and π^+ mesons) and thanks to the observation that the ε^{ToF} profile depends only slightly on the particle type, it was possible to apply these maps to the K^+, K^-, and $\phi \rightarrow K^+$, K^- decays.

The profile shown in fig. 3d in ref. [P1] indicates, that the MMRPC detector exhibits an excess of signals around its center or loss of hits at the sides. The analysis revealed that signals positioned around the center feature a clear excess of measured large clusters (groups of neighbouring active strips in a given module), and at the same time large clusters were concentrating nearly exclusively around the center. In searching for causes of these findings, I divided signals into 2 groups, large clusters and the other ones, and determined the distributions of topological variables for clusters: dispersion of time, position, and energy of the components of a cluster, and the degree of the geometrical linearity. However, these analyses did not reveal any distinguishable differences between these two groups, and thus they were abandoned, leaving only the trace in form of the presentation at the FOPI collaboration meeting.

Accounting for the ε^{ToF} efficiency contributed in smoothing out of the distributions of inverse slopes of K^+ and K^- mesons, which for the S325(e) experiment were reconstructed using two ToF detectors: MMRPC, and Plastic Barrel. It also caused an increase of extracted inverse slopes of transverse momenta of charged kaons to the level being in full agreement with the systematics at similar beam kinetic energies. An application of this additional efficiency raised the reconstructed ϕ meson yield per event by about 5 – 15%, which also influenced the value of the extracted α parameter of the power dependence of the ϕ meson yield on the number of collision participants, as described further in Subsection 5.1 of present Summary.

5. Physics results

5.1. Emission yields of hadrons in the collision

A most precise method of determination of the particle production yields per event is available for the high statistics samples acquired by the detection system within a wide scope of phase space. It is then possible to reconstruct the two-dimensional distribution of population of particles (in the coordinates of e.g. transverse momentum p_t and rapidity y), in order to parameterise it, and subsequently integrate. A typical example of the fenomenological distribution in a considered beam energy range is the Boltzmann-type function, parameterised in the $m_t - y$ or $p_t - y$ variables, which is fitted independly for subsequent rapidity slices. Another option is the Boltzmann-type function of energy multiplied by the expression parameterising the anisotropic emission in polar angle ϑ (both variables in the nucleon-nucleon (NN) frame).

A two-dimensional method was applied for the determination of the K^- and K^+ emission yields from the collisions of Ni+Ni at 1.91*A* GeV [P1,40], as well as protons and deuterons from the collisions of Al+Al at the same beam energy [26]. In the context of the Al+Al collisions I also collaborated in the K^+ meson yield reconstruction and am the main author of its description in the Subsection 4.3 of ref. [P2]. This method also allowed to obtain characteristic parameters of the

distributions, which will be reported in Subsection 5.4 of this Summary. The multiplicities per event obtained with help of this method are shown in Table 2 (systematic uncertainties follow the statistical ones). The Subsection 5.7 is devoted to the multiparametric procedure of estimation of systematic errors.

For the samples of lower statistics, a full two-dimensional phase space analysis is characterised by an instability of results, and a reduction of the number of degrees of freedom is necessary. It appeared to be the case during the analysis of the sample of about 2000 K^- mesons from the Al+Al collisions at 1.91*A* GeV, in which I collaborated. Events were projected into two one-dimensional distributions, kinetic energy and cosine of polar angle ϑ. The former distribution was fitted by the Boltzmann-type function, and the latter one – by the function parameterising the polar angle anisotropy. Distributions fitted in this way were subsequently mutually normalised, which allowed to reconstruct the total K^- emission yield, shown in Table 2.

For samples of even lower statistics the task of yield reconstruction requires a further reduction of the number of degrees of freedom. Results on particle yields determined with help of the method described below are shown in Table 3. A sample of ϕ mesons from central and semi-central Ni+Ni collisions (S325(e) experiment) was obtained by the analysis of the invariant mass distribution of K^+K^- pairs and amounted to about 170 events. For such a statistics, some insight into the one-dimensional kinetic energy distribution of ϕ mesons in the NN frame was possible (fig. 5 in ref. [P1]). A fit of the Boltzmann-type function to the obtained distribution allowed for its integration, and obtention of the ϕ meson emission yield, $[4.4 \pm 0.7\ ^{+1.6}_{-1.1}] \times 10^{-4}$. It is worthwhile noting, that lack of possibility to analyse the polar angle distribution results in inability to trace its

Table 2: Particle emission yields per triggered collision obtained with help of the two-dimensional phase space analysis.

System, energy	$\langle A_{part} \rangle_b$	Hadron	Yield per event	Ref.
Ni+Ni, 1.91*A* GeV	46.5 (*)	K^+	$[3.85 \pm 0.10] \times 10^{-2}$ (***)	[40] (preliminary)
		K^-	$[9.84 \pm 0.21\ ^{+0.33}_{-0.64}] \times 10^{-4}$	[P1]
Al+Al, 1.91*A* GeV	42.5	K^+	$[3.75 \pm 0.07\ ^{+0.33}_{-0.64}] \times 10^{-2}$	[P2]
		K^- (**)	$[9.5 \pm 1.0\ ^{+2.6}_{-0.1}] \times 10^{-4}$	[P2]
		p	21.00 ± 0.24	[26]
		d	4.00 ± 0.25	[26]

(*) Value published in [P1] was slightly corrected, and reported in ref. [P3].
(**) K^- yield obtained within the E_{kin}–ϑ projection method, cf. text below.
(***) Value is updated w/respect to that in ref. [40].

Table 3: Particle emission yields per triggered collision obtained with help of one-dimensional or inclusive signal analysis.

System, energy	$\langle A_{part} \rangle_b$	Hadron	Yield per event (*)	Ref.
Al+Al, 1.91*A* GeV	42.5	ϕ	$[3.1 \pm 0.5\ ^{+0.4}_{-0.8}] \times 10^{-4}$	[P2]
Ni+Ni, 1.91*A* GeV	46.5 (*)	ϕ	$[4.4 \pm 0.7\ ^{+1.6}_{-1.1}] \times 10^{-4}$	[P1]
Ni+Ni, 1.93*A* GeV	74	ϕ	$[8.6 \pm 1.6 \pm 1.5] \times 10^{-4}$	[P3]

(*) systematic uncertainties were obtained basing on different criteria. For the unified criterion, see Tab. I in ref. [P3].

possible changes in regions of phase space outside the acceptance of the FOPI setup. This lack of knowledge has to be accounted for in the statistical uncertainty, by checking the level of changes of the final result due to different assumed anisotropy coefficients of polar angle distribution given as input to the efficiency simulations. In case of the abovementioned analysis, a wide coverage of phase space by the ToF detectors of the FOPI setup caused this effect to be of minor importance.

A sample of ϕ mesons from the Al+Al collisions at the beam energy of 1.91*A* GeV consisted of even fewer events, about 108. My contribution to this research consisted in discussions of many aspect of analysis with the main author of ref. [P2] and co-authorship of the manuscript. For the case in question, the insight into the kinetic energy distribution of ϕ mesons was so limited, that integration of this distribution was not leading to convergent results. The only remaining method was then to divide the total number of ϕ meson events by the number of acquired Al+Al collisions, which had to be divided by the ϕ meson detection efficiency averaged over the whole window of FOPI acceptance in a given experiment. The reconstructed yield per collision was found to be $[3.3 \pm 0.5\ ^{+0.4}_{-0.8}] \times 10^{-4}$. This procedure is biased by the systematic uncertanties due to unknown characteristics of the kinematic distribution, and the assessment of these uncertanties was possible thanks to the estimations of possible ranges of these characteristics basing on available systematics.

After reconstruction of the sample of 110 ± 19 ϕ mesons from the central Ni+Ni collisions (S261 experiment), I applied the latter of reported methods, and determined the multiplicity of emission of these particles per collision. I reported on the analysis, and the obtained yield of $[8.6 \pm 1.6 \pm 1.5] \times 10^{-4}$ in ref. [P3].

Investigation of the ϕ meson production yield at the beam energy of 1.9*A* for three different systems of colliding nuclei allowed for the first time to obtain the dependence of the yield on the number of nucleons participating in the collision, $\langle A_{part} \rangle_b$, which is reported in fig. 4 of ref. [P3]. A parameterisation of this data with the power function yielded the exponent $\alpha = 1.8 \pm 0.6$ (systematic and systematic uncertainties were added quadratically). Due to the low statistics of samples, the obtained result is marked by the large uncertainty, which does not permit to formulate definite statements on the production scenario. One can be tempted to formulate two different hypotheses basing on the results: the linear, and the superlinear rise of yield with $\langle A_{part} \rangle_b$. The latter hypothesis may appear more probable, however, within 1.3 standard deviations the former scenario is possible as well. A superlinear rise with $\langle A_{part} \rangle_b$ is also a characteristic feature of K^+ and K^- emission around strangeness threshold [41]. For the positive kaons such a dependency was interpreted as a result of a considerable contribution of multi-step processes to their production (in particular with π meson or Δ baryon in the entrance channel) [22]. For the negative kaons, a similar $\langle A_{part} \rangle_b$ scaling is interpreted as a result of strong dependence of the K^- production on the appearance of K^+, required in order to conserve strangeness number $S = 0$ in the entrance channel ($NN \rightarrow NK^+Y \Rightarrow \pi Y \rightarrow K^-N$). A change of the character of dependency between the production yield and the number of participants from the linear to superlinear one was also observed while selecting the π mesons produced more and more close to the threshold in the NN channel [42]. These three cases may suggest, that if the dependency of ϕ meson production yield on the number of participants was strong, the multi-step channels could be among the prominent reasons. An additional suggestion in support of this hypothesis are the results of the calculations in the frameworks of the BUU and UrQMD models for the Ar+KCl system at the beam energy of 1.76*A* GeV, pointing to the dominance of the multi-step channels in case of this system [12,24].

On the other hand, calculations within the thermal model suggest, that due to the vanishing value of strangeness for the ϕ mesons, their multiplicity should be proportional to the volume of emission zone, and thus, to the number of participants [27]. As it was mentioned above, within the present statistics both hypotheses remain probable.

5.2. Yield ratios

By analysing the data from the Ni+Ni collisions at 1.9*A* GeV, I determined the ratios of ϕ/K^- production yields for the Ni+Ni collisions at 1.9*A* GeV. After addition of the value of this ratio from the Al+Al collisions, it became possible to inspect its dependence on the number of participant nucleons (cf. fig. 5a in ref. [P3]). It was found, that within the experimental uncertainties the $<A_{part}>_b$ dependence of this ratio is consistent with constant. Within such an assumption, the average ratio was found to be 0.36 ± 0.05. This value is nearly identical with the result for the Ar+KCl collisions at 1.76*A* GeV, equaling to 0.37 ± 0.13. It points to the stability of this ratio for a wider range of beam energies and colliding nuclei. Due to the branching ratio of BR ($\phi \rightarrow K^+K^-$) = 48.9% the results above translate into conclusion that 18% of K^- mesons originate from the decays of ϕ mesons. As majority of these decays occur in vacuum, the daughter negative kaons do not carry signatures of the modifications of hadron properties in nuclear matter. It means, that the procedures of extraction of the parameters of such modifications (e.g. the U_{KN} potentials) should account for this contribution. However, for the current predictions of the modifications of kaon properties, within the IQMD model this contribution was not included at all [1], and within the HSD model it was a few times underestimated. On the side of the UrQMD model, which does not include the in-medium modifications of kaon properties, calculations of the ϕ/K^- ratio were published this year. Results of these calculations are shown in fig. 5 in ref. [24]. They suggest that at the energies around threshold for the strangeness production the abovementioned ratio should be characterised by the pronounced maximum. For this range, the predictions were compared to the experimental results of the HADES group and of my analysis, and they turned out to be consistent within the experimental uncertainties.

Using the published yields of π^+ mesons, I also analysed the dependence of ϕ/π^+ ratio on the number of participant nucleons. As shown in fig. 5b in ref. [P3], two functions were fitted to the obtained data points, the constant, and the power one. They represent two predictions resulting from different assumptions. A constant value of this ratio is predicted in frame of the thermal model (cf. fig. 2 in ref. [27]), whereas the rise with the number of participants would correspond to the abovementioned hypothesis of the contribution of the multi-step channels in the subthreshold region of beam energies. The χ^2 value seem to prefer the power dependence scenario (the fitted exponent was found to be $\alpha = 1.0 \pm 0.6\ ^{+0.1}_{-0.0}$), but for the available statistics the other scenario remains probable as well.

5.3. Thermal model

An application of the thermal model for the heavy-ion collisions was outlined in Subsection 1.3. The yields of the emission of particles from the collision compared to the thermal model should be obtained (or scaled to) the same value of the number of participants, $<A_{part}>_b$. For the procedures of fitting of the thermal model predictions to the experimental particle yields I used the THERMUS package [31]. First results of an analysis for the ratios of yields of particles emitted from the Al+Al and Ni+Ni collisions are shown in fig. 4 in ref. [P6]. After determination of the ratio of deuteron to proton yields for Al+Al [26], I presented the updated fit result in ref. [P5]. A further determination of the emission yields of K^+, K^- and ϕ mesons for the Al+Al system allowed for a new, more exact update, shown in fig. 8 of this Summary. The latter fit was not published yet. The obtained parameters (T = 72.5 ± 1,1 MeV, and μ_B = 747 ± 5 MeV for Al+Al; T = 69 ± 12 MeV and μ_B = 760 ± 10 MeV for Ni+Ni) are in a quite good agreement with the systematics illustrated on the phase diagram of the nuclear matter in fig. 9.

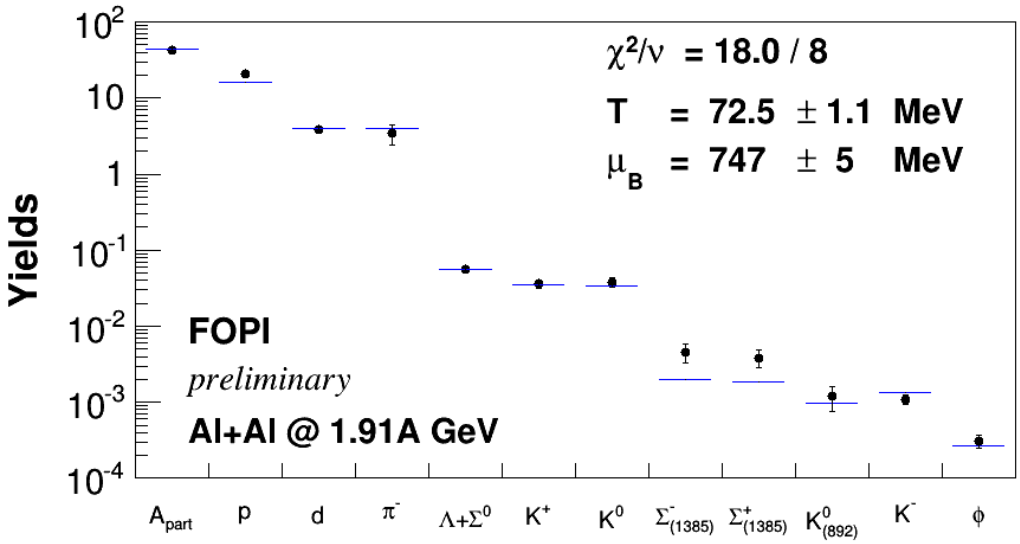

Fig. 8. Fit of the thermal model predictions (blue lines) to the reconstructed yields of the emission of hadrons from the collisions of Al+Al at the beam energy of 1.91*A* GeV (black points).

The abovementioned approach of applying the canonical ensemble for particles with the open strangeness implies that the volume in which these particles are produced (parameterised by the so-called canonical radius, R_C) is smaller than the volume of the collision zone. Within this approach the ratio of ϕ/K^- yields is sensitive to the value of R_C. The experimental values of the ϕ/K^- were reported above in this Summary, and are in agreement with the thermal model fit to the Ar+KCl system, presented in fig. 13 of ref. [25]. All the four data samples suggest that for the collisions of nuclei of the intermediate atomic masses, at the beam energies of 1.75 – 1.9*A* GeV the R_C radius should be within 2.2, and 3.2 fm.

5.4. Kinematic distributions

The distributions of population of particles in the phase space, dubbed the kinematic distributions, often exhibit noticeable deviations from the simple predictions of the Boltzmann model, which assumes the isotropic emission from the source being in thermal equilibrium. These deviations are the signatures of the collision process, which is influenced e.g. by the modifications of particle properties in the nuclear matter, effects of the collective expansion following the phase of condensation, and the final state interactions. In this context a relevant goal of the experimental approach is the reconstruction of distributions in broadest possible regions of phase space. Within my analysis I obtained the transverse momentum spectra for subsequent slices of rapidity, the distribution of inverse slope parameters as function of rapidity, and the rapidity distribution for K^- mesons from the Ni+Ni collisions at 1.91*A* GeV. These distributions were presented in fig. 4 and 5 in ref. [P1]. They are ready for comparisons with the theoretical predictions of the transport models, from where the scale of modifications of properties of charged kaons for the studied system can be estimated. I also determined the preliminary distribution of K^+ mesons in the phase space (a preliminary rapidity distribution is available in ref. [40]).

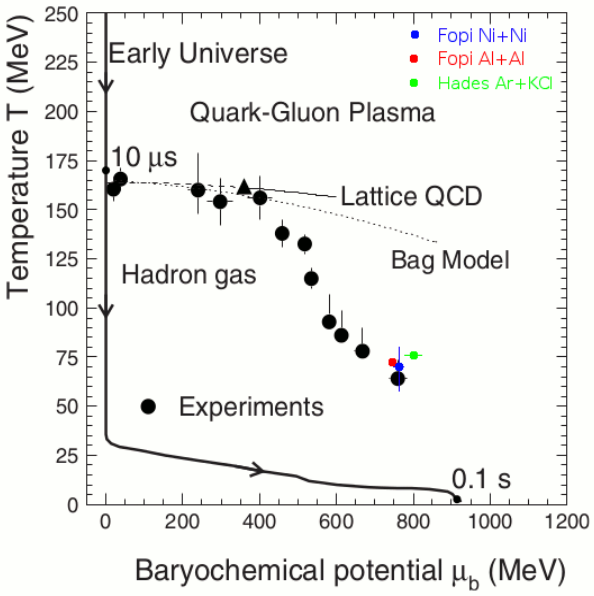

Rys. 9. Phase diagram of nuclear matter with results of the thermal model fits [43] to the particle emission yields from the collisions of Al+Al, Ni+Ni (1.9*A* GeV), and Ar+KCl (1.76 GeV) [49]

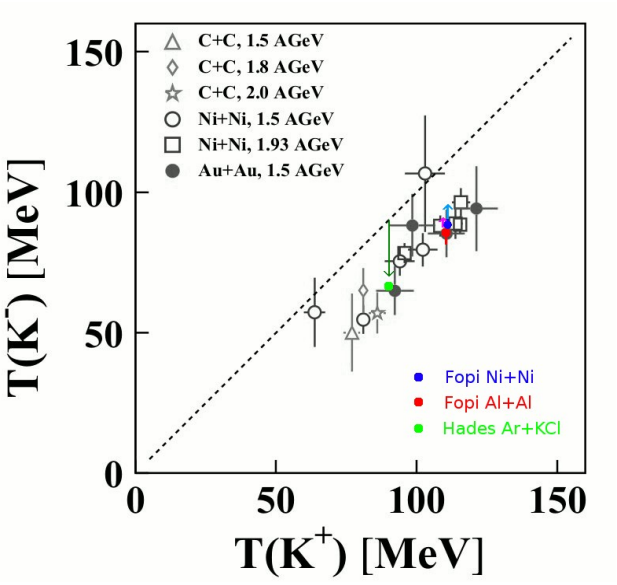

Rys. 10. Inverse slopes of kinetic energy spectra of K^+ and K^- mesons for heavy-ion collisions at the beam energies of 1.5 – 2.0*A* GeV. Results of the KaoS collaboration are shown in grey [28]; FOPI (Subsection 5.4): blue, and red; HADES: green. Inverse slopes for the *direct* components of negative kaons are shown with arrows (see text).

In case of study of distributions of charged kaons from Al+Al collisions at 1.91*A* GeV I participated in methodological discussions with the main author, dr P. Gasik, and an the main author of the description of these distributions, as enclosed in Section 4 of ref. [P2]. The parameters of inverse slope T and the anisotropy coefficient a_2 of the polar angle distribution fitted to the reconstructed distributions were reported in Table 2 of the abovementioned paper. In the next step the kinetic energy distributions of K^- and K^+ mesons were divided, and the results were compared to the predictions of the HSD transport model [44], assuming first the vanishing U_{KN} potential, and next its non-zero value. The results shown in fig. 9a of the considered paper evidence the existence of the in-medium modifications of properties of kaons and point to the values of about U_{K+N} = 40 MeV, U_{K-N} = –50 MeV. Regarding this analysis I co-authored its description in Section 6 of the paper. However, an extraction of the potential of K^- interaction with the nuclear matter would not be precise without accounting for the abovementioned contribution from ϕ meson decays. This issue will be described further in the Summary.

For the same colliding system I also determined the phase space distributions of protons and deuterons. The preliminary values of inverse slopes of transverse momentum distribution for the midrapidity in the NN frame were found to be $T_{y(NN)}$ (p) = 110 ± 7 MeV, and $T_{y(NN)}$ (d) = 105 ± 5 MeV, respectively. The values of inverse slope were first published in ref. [26], and after further corrections they joined the collection of data points presented in fig. 3 of ref. [P6]. If the emission of each of protons and deuterons was described by the Boltzmann distribution with temperature equal to the found inverse slope T, the rapidity distribution should be characterised by the Gaussian profile, as indicated by the dashed line in fig. 1 in the abovementioned paper. However, the experimental rapidity distributions presented in this figure exhibit a very pronounced elongation with respect to the predictions of the Boltzmann model. It is a characteristic feature of rapidity distributions of the emission of protons and light fragments in the considered range of beam

energies, being the result of the partial transparency in the interpenetrating nuclei in the course of the collision [28,45].

A detection of ϕ mesons in samples amounting to about 100 – 200 events allowed for some insight into their distributions of kinetic energy. Following the first such distribution published by the HADES group [25], my analysis of the sample from semi-central and central Ni+Ni collisions (S325(e) experiment) allowed for extraction of the second distribution of this type, presented in fig. 5 of ref. [P1], and determination of the inverse slope of T = 106 ± 18 (stat) $^{+18}_{-14}$ (syst) MeV. I am also the main author of the description of the reconstruction of kinetic energy distribution of ϕ mesons from the Al+Al collisions, performed by dr. P. Gasik, and enclosed in Section 5 of ref. [P2]. In this case the inverse slope parameter was found to be T = 93 ± 14 $^{+17}_{-15}$ MeV. Unfortunately, the analysis of the sample of ϕ mesons from central Ni+Ni collisions (S261 experiment) revealed an instability of the extracted T parameter, and therefore was not presented.

5.5. Two-source model of distribution of K^- emission

The studies presented above resulted in conclusion, that the measured K^- mesons originate from two sources: a dominant contribution from the collision zone, which carries traces of in-medium modifications of kaon properties (so-called ”*direct*” contribution), and a contribution from ϕ meson decays, occuring mainly in vacuum – properties of such kaons are not modified (”ϕ” contribution). Having the experimentally determined yields of K^- and ϕ mesons, and the inverse slope parameters T of their transverse momentum or energy distributions (in the K^- case it is the inclusive distribution), one can search for the characteristics of the *direct* contribution of K^- mesons. The first study of this kind was reported in ref. [46] for the Ar+KCl system at the beam energy of 1.76*A* GeV. In that analysis, the question was posed if it is posible to explain the superiority of $T(K^+)$ over $T(K^-)$ by assumption that the inverse slope of the *direct* component of K^- mesons is equal to $T(K^+)$, and the factor that makes the effective slope lower is the contribution from the ϕ meson decays. The preliminary answer was positive within the statistical uncertainties (c.f. green arrow in fig. 10). This result has put in question the previous interpretation of the effect of larger values of $T(K^+)$ compared to $T(K^-)$ as the result of opposite signs of potentials of interaction of different kaons with the surrounding matter (U_{K+N} and U_{K-N}). Thus, a question arose, what are the relative weights of two competing phenomena: the potential effect, and the effect of feeding from ϕ meson decays. Only a thorough analysis of the experimental data can answer this question.

For the semi-central collisions of Ni+Ni (S325(e) experiment), having the inverse slope T of ϕ mesons, and assuming the isotropic distribution of their emission, I employed the PLUTO[47] package to simulate decays of these mesons into K^+K^- pairs, and obtained the distribution of inverse slopes $T_{K^-,\phi}$, shown in triangles in fig. 6 of ref. [P3]. They are apparently lower than the inverse slopes of the inclusive K^- spectra, i.e. the fits of the single Boltzmann-type function to the experimental K^- distributions, denoted by the empty squares. A fit to the transverse momentum spectra of the sum of two contribution (*direct* and *ϕ*), weighted according to the experimentally obtained value of ϕ/K^- ratio allowed to extract the distribution of inverse slopes for the *direct* contribution, as denoted by the empty circles. The latter slopes are found to be higher by about 10 MeV than the inclusive values (although an estimation of the systematic errors is missing in this analysis). By comparing this result to the T (K^+) – T (K^-) difference, measured for the NN midrapidity, and found to be about 25 MeV [15], one can infer that the potential effect and the effect of feeding from ϕ mesons may contribute to a similar extent in creation of this gap (cf. blue arrow in fig. 10).

With dr. P. Gasik, we performed the similar analysis for the Al+Al system, which was reported in ref. [P2]. My contribution was the simulation of ϕ meson decays in the K^+K^- channel for the experimentally extracted value of T for the ϕ mesons, which allowed to obtain the inverse slope of the energy distribution of daughter negative kaons. I also contributed to the physics discussion and co-authored the description of the analysis in Subsection 6.2 of that paper. The obtained value of the inverse slope of the *direct* contribution of the K^- mesons was found to be $89 \pm 9\ ^{+24}_{-11}$ MeV: somewhat higher than the value obtained in the inclusive fit of the K^- energy spectrum, $82 \pm 6\ ^{+21}_{-6}$ MeV, but also lower than the value of T describing the inverse slope of the K^+ energy spectrum, $109 \pm 2\ ^{+6}_{-13}$ MeV (note that the systematic uncertainties do not permit to consider these hints as final conclusions). The results of this analysis constitute another suggestion that the gap between $T(K^+)$ and $T(K^-)$, observed for several colliding systems, may not be exclusively caused by the potential effect, but also by the feeding from ϕ meson decays (cf. purple arrow in fig. 10).

All the above results suggest the necessity of including the ϕ mesons in extracting information on the modifications of properties of K^- mesons in the nuclear matter. As for the extraction of this information the transport models are employed, they should either correctly describe the production of these mesons, or the comparisons between experimental data and model predictions should be performed after removal of the contribution from ϕ meson decays from distributions of K^- mesons. The latter approach was chosen for the Al+Al case, and my role was the participation in the physics discussion and co-authorship in the description of the analysis at the end of Subsection 6.2 of ref. [P2]. The distribution of ratio of kinetic energy distributions of K^- to K^+ after removal of the ϕ contribution is presented in fig. 9b therein. It is characterised by somewhat lower values and a flatter profile, than in the inclusive case, shown in fig 9a. The obtained result suggest, that the value of $U_{K-N} = -50$ MeV, extracted for the inclusive case, is overestimated. It constitutes a suggestion for the theoretical groups to improve the model calculations in the considered scope, and repeat some of calculations for the considered colliding systems.

5.6. Parameterisation of $T(m)$ dependence with radial flow

The distribution of inverse slopes T of kinematic distributions of particles in the NN midrapidity as function of particle mass m, shown in fig. 3 of ref [P6], may suggest the rise of T with mass. Such a scenario is possible within the assumption that the kinetic energy of motion of particles is composed of two terms: the thermal part, $^3/_2\,T$, and the non-relativistic term describing the collective radial expansion, $\frac{1}{2}\, m(\beta_{rad}c)^2$, where $\beta_{rad}c$ is the velocity of radial flow [48]. Such a description may give rise to doubts regarding its rightness. It does not account for the specifics of nucleons – as particles existing before the collision, mesons and strange baryons – as particles producted in course of the collision thanks to the available energy in the energy balance od channels, and light fragments – as possible products of coallescence of nucleons, or originating from the fragmentation of spectators. The abovementioned parameterisation also does not explain the difference of K^+ and K^- slopes, discussed in the previous Subsection of this Summary (cf. fig. 10). However, this model can be treated as a practical parameterisation of the inverse slopes of particles, and some approximation of the description of the collision dynamics. A fit of its predictions to the inverse slopes of particles emitted from Al+Al (Ni+Ni) collisions is shown in fig. 3 of ref. [P6], and points to the temperatures of 88 (105) MeV, and radial flow velocities of $0.17c$ ($0.25c$), respectively. It is worthwhile noting, that the abovementioned temperatures, resulting from the analysis of kinematic spectra (so-called *kinetic temperatures*) are noticeably larger than the values of T obtained basing on the fits of the thermal model to the particle yields (so-called *chemical temperatures*, cf. Subsection 5.3). A phenomenon of superiority of the kinetic temperatures over the chemical ones in the beam energy range of 1 – 2A GeV was also observed in

the collisions of Ar+KCl at the beam energy of 1.76*A* GeV (cf. fig. 9 of ref. [49]). It is an unexpected observation. In the collisions at higher beam energies an inverse hierarchy of temperatures was observed (cf. figs. 3 and 4 in ref. [27]), which was interpreted as a result of precedence in time of stabilisation of the particle emission yields (*chemical freeze-out*) over stabilisation of the profiles of kinematic distributions (*thermal* or *kinetic freeze-out*). These findings observed in heavy-ion collisions at the beam energies of 1.5 – 2*A* GeV could either point to possible flaws of the thermal approach as the model aiming to describe the distributions of particle emission from heavy-ion collisions, or to oversimiplified assumptions of the parameterisation of dependence between inverse slope and the particle's mass.

5.7. Estimation of systematic uncertainties

A number of factors contributed to the estimation of systematic uncertainties of the obtained results. First of all it is worthwhile to mention an assessment of sensitivity of results to small variations of parameters relevant for track quality in the CDC chamber, and for matching of these tracks with the hit points in the ToF detectors. For the analysis of distributions of $K^{\pm}$ mesons it was crucial to assess the influence of binning of phase space in histograms, of an assumed range of fitting the transverse momentum distributions, and of the strategy of extrapolation of the rapidity distrbution outside the detector acceptance region. For the investigation of ϕ mesons the considered factors were systematised in Table II of ref. [P3]. In case of the analyses reported in refs. [P1] and [P2], for each of parameters playing role in the abovementioned tasks I defined the relevant range, and probed it with 2 to 5 intermediate values. Subsequently, I stored the physical quantity X for all the combinations of considered parameters, which built the distribution $f(X)$ of possible values of X. It allowed to identify the experimental value of X as the average of this distribution, and made possible to define the confidence level (CL) at which the systematic uncertainty is to be given. For the analysis in ref. [P2] dr. P. Gasik applied a different strategy: the abovementioned contributions to the systematic uncertainties were considered, but the systematic uncertainties were defined as those including the whole range of variations of the investigated quantity X.

III Other research activity

1. Activity within the TAPS Collaboration

In years 2000 – 2010, i.e. during my M.Sc. research, Ph. D. research and at the beginning of work as an associate professor, as a member of the TAPS Collaboration I performed analyses of the photon and π^0 meson emission from heavy-ion collisions at intermediate beam energies, in particular at 40*A*, and 60*A* MeV. In this range, with an increase of the beam energy the nucleon excitation energy passes from values below the binding energy of nucleon inside nucleus (about 8 MeV) toward higher values. In addition, the dynamics of colliding nuclei depends on the degree of collision centrality. For the peripheral collisions, fragments of excited quasiprojectile and quasitarget emerge, which subsequently deexcite through evaporation. In case of semicentral collisions, a neck structure appears in the contact zone of colliding nuclei, and subsequently all the components disintegrate in course of the multifragmentation process. For the central collisions the system undergoes condensation and, depending on the beam energy, may either disintegrate through multifragmentation, or even undergo complete disintegration to the light particles. Due to strong changes of collision topology, it is crucial to obtain experimental information on the shape of the

collision zone of heavy-ions. One of possible methods is the technique of correlation function of pair of particles.

For the analysed experiments the TAPS detection system consisted of 6 blocks covering wide range of polar angles, ϑ (45° – 135°) , and composed of BaF_2 scintillation modules, and the KVI Forward Wall placed downstream (FW; $\vartheta \in$ (2.5° – 25°)), composed of plastic scintillation modules. Thanks to the choice of active materials, the TAPS system allowed for the detection of photons (and reconstruction of their energy and angular distribution), and the measurement of charged particles emitted emitted in forward directions (and estimation from it the degree of centrality).

Photons are neither hadrons nor leptons, and have no electric charge, therefore their distributions in phase space carry an unbiased information on the source of their emission. In the considered range of beam energies the probability of emission in a collision of a $\gamma\gamma$ pair originating from two independent acts of bremsstrahlung is comparable to the probability of a $\gamma\gamma$ pair from the decay of π^0 meson (BR $\approx$ 99%). As these two groups of $\gamma\gamma$ pairs can be separated to a large extent using the invariant mass, for the bremsstrahlung $\gamma\gamma$ pairs one may attempt to obtain the correlation function C_2. Within the HBT interferometry method, the Fourier transform of an excess of C_2 over the value of 1 at lower momentum (energy) differences, is identical to the space-time distribution of the particle source. The leading topic of my Ph.D. research was the interferometry analysis of the $\gamma\gamma$ pairs from Ta+Au collisions at the beam energy of 40*A* MeV, which I performed together with the data calibration, clusterisation of signals and rejection of background originating from electrons and particles of cosmic radiation. In the first step I obtained the correlation function against the invariant mass for the collisions of inclusive centrality. The result shown in fig. 2 of ref. [50] does not exhibit the interference signal. Subsequently, data were divided into classes of collision centrality, whose degree increases with the number of charged particles in the FW detector. In the class of central collisions thte C_2 function, shown in fig. 4 therein suggests a probability for an interference signal. However, the statistics of $\gamma\gamma$ pairs turned out to be insufficient for confirmation of this signal at the level above 3 standard deviations. On the other hand a fit of the Gaussian function to the data allowed for extraction of the „space-time radius", which was found to be 10.3 ± 2.7 fm. This radius incorporates the mixed information on the space and time dimensions of the source. A separation of these dimensions should be possible through the analysis of the C_2 function on the two-dimensional space of difference of photon energies q_0, and difference of their momenta, $|\bar{q}|$. However, the insufficient statistics of the $\gamma\gamma$ pairs did not permit for an analysis of the signal on more than one dimension.

The analysis of energy distributions of single photons for the abovementioned system of colliding nuclei, performed by me, showed that the high-energy part in these distributions cannot be described by one Boltzmann-type function, but it can be parameterised by the sum of two functions of this kind, characterised by different values of inverse slopes. For the studied system of colliding nuclei the ratio of integrated intensities of high-energy to low-energy contribution was found to be 2.2 ± 0.3 for all the centralities inclusively (and it grew with degree of collision centrality), whereas the inverse slopes of these contributions were found to be 13.0 ± 0.2 MeV, and 5.1 ± 0.3 MeV respectively. These results evidence that the source of photon emission has an internal structure, a statement also supported by the results for other colliding systems, and results of calculations in the framework of the BUU transport model [51]. The latter results suggested the sequential scenario, where after the initial condensation of matter (and emission of most energetic photons) it is diluted, and subsequently recompresses (and the photons are emitted once more, this time carrying on average less energy). However, such a scenario implies that the model of source of $\gamma\gamma$ pairs should be extended. If the sample of $\gamma\gamma$ pairs was several times more abundant, an extraction of relevant model parameters from data would be possible.

Another branch of my research was the analysis of π^0 meson emission. Beam energy of about 40 – 60*A* MeV constitutes merely about 15 – 20% of the threshold energy for the production

of π^0 meson in the NN channel, therefore the production of these particles is deeply subthreshold. Within the M.Sc. research and in the beginning of my Ph.D. I obtained the inverse slopes *T* of transverse momentum distributions of these mesons from the collisions of Ar+C, Ni, Ag and Au at the beam energy of 60*A* MeV. Within experimental uncertainties all these values of slope were in mutual agreement, and the average slope equalled to 15.6 ± 0.8 MeV. An independence of the inverse slopes from the size of colliding system is consistent with the assumption that the π^0 meson production occurs during the primordial NN collisions, where the available energy is formed by the superposition of two vectors: beam momentum, and momentum of Fermi motion of nucleons in target and beam nuclei [52]. In the beginning of my duties as an assistant professor, I also reconstructed the distributions of transverse momentum, energy, and polar emission angle in the NN frame for the π^0 mesons from the Ta+Au collisions at even lower beam energy, 40*A* MeV. As shown in figs. 3a, and 5a of ref. [53], the energy and transverse momentum distributions obtained for this system cannot be described by the Boltzmann-type function. If this function is fitted to the high-energy tail of these distributions, the inverse slope parameter is found to be about 9 – 10 MeV. The reconstructed polar angle distribution exhibited a small anisotropy: if the phenomenological function $dN/d\Omega \sim 1 + a_2 \cdot \cos^2 \vartheta_{NN}$ is fitted to the data, the value of a_2 parameter is found to be 0.31 ± 0.09.

The TAPS group has developed the simplified model of absorption of π^0 mesons emitted in the heavy-ion collisions [54]. Within this model the attenuation functions of the neutral pion yield were calculated as function of their energy, transverse momentum and the polar emission angle. Dividing the experimental distributions by the respective attenuation functions allows to estimate the distributions of primordial pions (before the absorption). The angular distribution of primordial pions reconstructed within this absorption model turned out to be in agreement with the isotropic scenario ($a_2 = 0.09 \pm 0.09$). The distributions of transverse momentum and energy of primordial pions are reported in figs. 3b and 5b of ref. [53]. These distributions were found to disagree with the Boltzmann profile as well.

An important step toward the identification of the π^0 meson production process in the abovementioned colliding system was finding that their energy distribution goes far beyond the kinematic limit of the $NN \rightarrow NN\pi^0$ channel, even taking into account the constructive superposition of momenta of the Fermi motion of nucleons. With help of the PLUTO package I performed the simulations of two scenarios of π^0 meson production: via the $NNN \rightarrow NNN\pi^0$ channel, and via the two-step $NN \rightarrow N\Delta$, $\Delta N \rightarrow NN\pi^0$ channel. For both cases the limit of the energy distribution of produced neutral pions nearly matched the experimentally observed limits of π^0 energies. Therefore, these production channels appear to explain the high-energy tail of the experimental distribution of π^0 mesons produced at the beam energy of 40*A* MeV.

2. Activity within the CBM Collaboration

During the first years of my duty as an assistant professor I performed for the CBM Collaboration the symulations of placement of a detector dedicated to muons from the J/ψ meson decays. The CBM is the experimental setup to be operating at the SIS100 accelerator at the GSI, Darmstadt, both facilities being currently under construction. The aim of the SIS100 accelerator is to deliver beams of heavy-ions of energies from 2 to over 10 *A* GeV [55]. In the longer term planned is the construction of another accelerator, SIS300, which would broaden the range of available beams to few tens of *A* GeV (35*A* GeV for the Au beam). Among the research goals of the CBM group, apart from studies of the global characteristics (nuclear matter equation of state, phase transition to the quark-gluon plasma, and restoration of the chiral symmetry), one also plans to investigate the rare signals, e.g. hadrons with c or b quark. In this context the goal of our study was to search for the most favourable solution for detection of the J/ψ mesons (composed of $c\bar{c}$ pairs), in

the selected decay channel of $J/\psi \rightarrow \mu^+\mu^-$ (BR $\approx$ 6%). In a group of correlated pairs of muons of opposite signs from heavy-ion collisions, a considerable part originates from decays of $\pi^{\pm}$ mesons ($\pi^{\pm} \rightarrow \mu^{\pm}$) occuring on the particle paths toward the detectors. For the investigation of J/ψ mesons these pairs constitute a considerable background.

Within the designed CBM experimental setup one plans to install the multi-layer vertex detectors (MVD, and STS), surrounded by the superconducting dipole magnet. At a few-meter distance behind the target the TRD detector is planned to be installed, followed by the TOF detector and, subsequently, the ECAL calorimeter, the latter ones in form of the forward wall. As an option, an installation of the movable RICH detector is considered between the last TRD layer and the first TRD wall. In one of the propositons dedicated to studies of the $J/\psi \rightarrow \mu^+\mu^-$ decays it was suggested to mount in the same place the movable detector composed of series of alternate thick absorbers and detection layers (so-called Muon Chamber, MuCh). Whereas the signal to background ratio (S/B) was expected to be favourable, the disadvantage was the absorption of clear majority of emitted hadrons, causing that the experiments dedicated to the J/ψ studies would have to be nearly exclusive.

The first solution from the Warsaw branch of the CBM group was the placement, as an alternative, the new muon detector at the end of the setup, behind the ECAL plane. Our initial step was the search of placement and size to be most favourable with respect to S/B, level of significance ($S_2 = S / \sqrt{(S+B)}$), and costs of manufacturing. The simulations were carried out within the CbmRoot framework, which incorporated the Geant3 package. As an input we chose the events of Au+Au collisions at the energy of 25*A* GeV, generated by the UrQMD transport model, whereas the J/ψ mesons were generated by the Pluto package and added to the events. Basing on the result of our simulation we proposed the setup composed of two vertically placed rectangular walls, centered at the polar angle $\vartheta = 12.5^{\circ}$ one placed above, and one below the beamline. A single wall would span the area of 25 m^2, and the ratio of the horizontal to the vertical side would equal to 1.7. In the next step, in the context of the multiple scattering on the path between the last STS layer and subsequent TRD walls, we analysed the distributions of deviation of the point of particle's hit in the TRD wall from the expected extrapolation from previous layers. It turned out that the muons originating from the $\pi^{\pm}$ decays, which constituted the background, are characterised by a clearly larger deviation than these from the decays of J/ψ mesons in the target. Thanks to our cuts on the maximum value of these deviations the S/B increased by 2–3 times to the value of 0.5. I reported on the abovementioned analysis at the 8th CBM Collaboration Meeting in Strasbourg in September 2006, and in the CBM Progress Report 2006 [56]. Although the advantage of the proposed solution compared to the MuCh chamber was not blocking by the dedicated detector the measurements of other phenomena during the experiment, the results obtained by the MuCh exhibited clearly higher S/B ratio of the value of 7.

The second proposition of the Warsaw CBM group was an insertion of the absorbers between subsequent TRD walls. Such a configuration was shadowing the further CBM detectors, but was enabling the simultaneous measurement of emitted particles by the RICH detector and the 1st TRD layer. However, the preliminary results of the simulation for the J/ψ decays in the $\mu^+\mu^-$ channel suggested the low S/B value of 0.02. I reported on this research on the XI CBM Collaboration Meeting in February 2008 at the GSI, Darmstadt. Due to the necessity of intensive works within the FOPI Collaboration, the simulations of the CBM detector were discontinued.

IV The bibliography

[1] C. Hartnack et al., Phys. Rep. 510, 119 (2012).
[2] B. Hong et al., Phys. Lett. B 407, 115 (1997).
[3] W. Reisdorf et al., Nucl. Phys. A 781, 459 (2007).
[4] W. Reisdorf et al., Nucl. Phys. A 848, 366 (2010).
[5] A. Andronic et al., Nucl. Phys. A 772, 167 (2006).
[6] M.C. Birse, J. Phys. G: Nucl. Part.Phys. 20, 1537 (1994).
[7] D.B. Kaplan, A.E. Nelson, Phys. Lett. B 175, 57 (1986).
[8] W. Weise, Nucl. Phys. A610, 35c (1996).
[9] T. Waas et al., Phys. Lett. B 379, 34 (1996).
[10] K. Tsushima et al., Phys. Lett. B 429, 239 (1998).
[11] J. Schaffner-Bielich et al., Nucl. Phys. A 625, 325 (1997).
[12] H. Schade et al., Phys. Rev. C 81, 034902 (2010).
[13] M.F.M. Lutz, Prog. Part. Nucl. Phys. 53, 125 (2004).
[14] M. Kotulla et al., Physik Journal 8, 3, p. 41 (2009).
[15] A. Förster et al., Phys. Rev. C 75, 024906 (2007).
[16] A. Mangiarotti et al., Nucl. Phys. A 714, 89 (2003).
[17] M. Merschmeyer et al., Phys. Rev. C 76, 024906 (2007).
[18] X. Lopez et al., Phys. Rev. C 81, 061902(R) (2010).
[19] X. Lopez et al., Phys. Rev. C 76, 052203(R) (2007).
[20] K.A. Olive et al., Chin. Phys. C, 38, 090001 (2014).
[21] C.B. Dover, G.E. Walker, Phys. Rep. 89, 1 (1982).
[22] C. Fuchs, Prog. Part. Nucl. Phys. 56, 1 (2006).
[23] B. Borasoy et al., Eur. Phys. J. A 25, 79 (2005).
[24] J. Steinheimer, M. Bleicher, J. Phys. G: Nucl. Part. Phys. 43, 015104 (2016).
[25] G. Agakishiev et al., Phys. Rev. C 80, 025209 (2009).
[26] K. Piasecki et al., GSI Scientific Report 2010, p. 66, GSI (2011).
Url: http://repository.gsi.de/record/53521/files/GSI-Report-2011-1.pdf
[27] J. Cleymans, K. Redlich, Phys. Rev. C 60, 054908 (1999).
[28] G. Wolf et al., Prog. Part. Nucl. Phys. 42, 157 (1999).
[29] E.L. Bratkovskaya et al., Nucl. Phys. A681, 84c (2001).
[30] F. Becattini et al., Eur. Phys. J. C 5, 143 (1998).
[31] S. Wheaton et al., Comp. Phys. Comm. 180, 84 (2009).
[32] J. Ritman, Nucl. Phys. (Proc. Suppl.) B 44, 708 (1995).
[33] B. Sikora, Acta Phys. Pol. B 31, 135 (2000).
[34] K. Wiśniewski et al., Eur. Phys. J. A 9, 414 (2000).
[35] M. Kiš et al., Nucl. Instr. Meth. A 646, 27 (2011).
[36] A. Schüttauf et al., Nucl. Instr. Meth. A 602, 679 (2009).
[37] V. Zinyuk et al., Phys. Rev. C 90, 025210 (2014).
[38] J. Gosset et al., Phys. Rev. C 16, 629 (1977).
[39] wwwasdoc.web.cern.ch/wwwasdoc/geant_html3/geantall.html
[40] K. Piasecki et al., GSI Scientific Report 2009, p. 230, GSI (2010).
Url: http://repository.gsi.de/record/53522/files/GSI-Report-2010-1.pdf
[41] R. Barth et al., Phys. Rev. Lett. 78, 4007 (1997).
[42] C. Müntz et al., Z. Phys. A 357, 399 (1997).
[43] P. Braun-Munzinger, J. Wambach, Rev. Mod. Phys. 81, 1031 (2009).
[44] W. Ehehalt et al., Nucl. Phys. A 602, 449 (1996).
[45] W. Reisdorf et al., Phys. Rev. Lett. 92, 232301 (2004).
[46] M. Lorenz, PoS (BORMIO2010) 038 (2010).
[47] I. Froelich et al., PoS ACAT2007, 076 (2007).

[48] P.J. Siemens, J.O. Rasmussen, Phys. Rev. Lett. 42, 880 (1979).
[49] G. Agakishiev et al., Eur. Phys. Jour. A 47, 21 (2011).
[50] K. Piasecki, T. Matulewicz, Acta Phys. Pol. B 37, 1 (2006).
[51] G. Martínez et al., Phys. Lett. B 349, 23 (1995).
[52] K. Piasecki et al., Acta Phys. Pol. B 33, 973 (2002).
[53] K. Piasecki et al., Phys. Rev. C 81, 054912 (2010).
[54] K. Tymińska et al., Acta Phys. Pol. B 33, 981 (2002).
[55] J. Heuser et al., Nucl. Phys. A 904, 941c (2013).
[56] K. Piasecki et al., CBM Progress Report 2006, 20 (2007).
Url: http://repository.gsi.de/record/54085/files/GSI-2013-04807.pdf